A Comprehensive Algorithm for Estimating Lithium-Ion Battery Parameters From Measurements

Dominik Dvorak, Thomas Bäuml, Alexandra Holzinger, and Hartmut Popp

***Abstract*—The use of equivalent circuit models for simulating the operating behavior of lithium-ion batteries is well established in the automotive and the renewable energy sector. However, finding the correct parameter set for these models is still a challenging task. This manuscript proposes a comprehensive methodology for estimating the required, temperature dependent simulation parameters from battery measurements. Based on a specific load current and prior system knowledge, an algorithm first analyses the correlation between current steps and the measured terminal voltage. Second, a combination of particle swarm optimization and Gauss–Newton algorithm fits the initially estimated parameters from the first algorithm to the measurement data. Finally, the dependency of each simulation parameter on both the state of charge and the battery temperature is determined. As this contribution aims at modeling reversible effects of lithium-ion batteries, ageing effects are neglected. The validation against measurement data proves that the generated parameter set enables the user to accurately reproduce and investigate the operating behavior of the chosen battery. Applied to a lithium-iron-phosphate cell, the comparison between measurements and simulations in standardized real-life automotive driving cycles (Artemis, FTP75 and WLTC) shows a terminal voltage error of less than 1.09% within the typical operational window between state of charge 0.15 and 0.95.**

***Index Terms*—Lithium-Ion battery, electrical equivalent circuit, parameter estimation, particle swarm optimisation, Gauss-Newton algorithm.**

I. Modeling and Simulation

THE use of mathematical- or electrical equivalent circuit (EEC) models for simulating the operating behaviour of different types of batteries is already well-established in the automotive and the sustainable energy sector [1]–[8]. This method offers a good trade-off between accuracy of the simulated operating behaviour and simulation speed [9]. This is an important argument, especially when a high number of cells need to be simulated with good time resolution over longer periods, like in case of electric vehicles or stationary applications.

However, despite all advantages such simulation models are often difficult to parametrise. Although there are some approaches available, it is still a challenging task to get the parameters for EEC models for simulating the operating behaviour of specific Lithium-Ion batteries conveniently. Furthermore, the parameters of the EEC should be dependent on the state of charge (SOC) and the temperature (T) for such a type of simulation. For creating a simulation model that achieves short simulation times and high accuracy, the parameters variability is described as function $f(\mathrm{SOC},\ \mathrm{T})$ and not as look-up tables because the solver of the simulation tool can handle functions more accurately and efficiently and less data points have to be stored.

Estimating parameters for batteries and for Lithium-Ion batteries in particular is a topic which received a lot of attention over the last decade [1], [3]–[7]. Waag *et al.* [10] identified over 350 publications concerning this topic in their review paper. A high number of different approaches is found in this review, while only one author [11] proposes the use of a Particle Swarm Optimisation (PSO) method for identifying EEC parameters, in this case for online diagnostics. Since then, some authors implemented the PSO for finding EEC parameters [12], [13] and also to find electrochemical parameters [14]. In these articles PSO is proven to bring reliable results for this field of application, but it needs high computational power to achieve high accuracy [10]. The Gauss-Newton (GN) algorithm is used for fitting EECs, for example to compare models of different complexity [15] or to gain electrochemical parameters [16]. In their work Reuter *et al.* [17] compare different optimisation methods. In this comparison the GN is found to be very accurate for estimating the parameters of a Lithium-Ion battery but can be rather slow or requires high computational power, respectively. Another drawback is that the GN can get stuck in a local minimum. To overcome the drawbacks of each optimisation algorithm, in this work firstly a PSO is used for getting near the global optimum of the parameters. Subsequently, the estimation of the global optimum of the PSO is refined by a GN algorithm. By applying this combined approach, accurate results can be achieved while keeping the computing time low. Shen *et al.* [18] proofed this method to be suited for battery parameter estimation by combining a PSO with a Levenberg-Marquardt algorithm to gain electrochemical parameters like potential and current density. However, in their model they neglect the temperature dependency of the parameters, which is one of the main innovations of this work. Furthermore, the authors of [18] follow an electrochemical approach, while this work uses an EEC for modelling Lithium-Ion batteries.

II. Equivalent Circuit Models

Fig. 1 shows typical EECs for modelling the electrical operating behaviour of Lithium-Ion batteries at different levels of complexity. The models can be used to calculate the terminal voltage v_{sim} of the battery.

The simplest model a) considers an open circuit voltage (OCV) which represents the potential between the two

Manuscript received April 20, 2017; revised August 29, 2017; accepted September 29, 2017. Date of publication December 25, 2017; date of current version March 20, 2018. Paper no. TSTE-00352-2017. *(Corresponding authors: Dominik Dvorak.)*

The authors are with the AIT Austrian Institute of Technology GmbH, Vienna 1210, Austria (e-mail: dominik.dvorak@ait.ac.at; thomas.baeuml@ait.ac.at; alexandra.holz@gmx.at; hartmut.popp@ait.ac.at).

Digital Object Identifier 10.1109/TSTE.2017.2761406

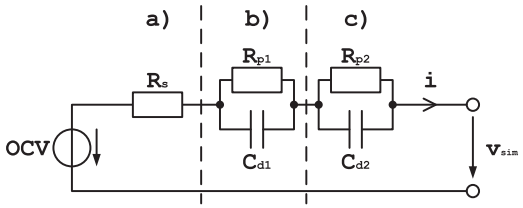

Fig. 1. Different electrical equivalent circuit models for Lithium-Ion batteries.

electrodes if no current is withdrawn from the battery. If a load current is applied to the battery, the series resistance R_s considers the immediate ohmic voltage drop due to the resistance of the electrolyte, the pins and the active material. However, the strongest influence arises from the electrolyte [8].

The EEC shown in Fig. 1 b) consists of the same components as a), but with an additional RC-parallel circuit element connected in series. This allows to consider transient voltage effects such as transition effects between ionic and electrical conductance and double-layer effects [8]. The time constant for these effects is within the range of seconds and can be calculated by $\tau_1 = R_{p1}C_{d1}$.

The third EEC, which is shown in Fig. 1 c), considers the same effects as b), but with a second RC-parallel circuit element connected in series. This element allows to consider long-term transient effects like the relaxation effect [19]. The time constant for this process is within the range of several minutes and can be calculated by $\tau_2 = R_{p2}C_{d2}$.

The OCV of the battery strongly depends on the SOC. Therefore, a voltage hysteresis, which is the gap between the charge- and discharge curve, must be considered. It is more distinct for Lithium-Iron-Phosphate (LFP) cells than for cells with other cathode materials, such as Nickel-Manganese-Cobalt (NMC) [8]. Therefore, hysteresis is considered and the OCV is not only a function of the SOC but also dependent on the direction of the current flow.

The parameter estimation algorithm presented in this contribution focuses on the EEC c). The algorithm can be adjusted to fit the circuits b) or a) by simply neglecting the voltage drop at one or both RC-parallel circuit elements, respectively. In the following chapter the measurements, which form the basis for extracting the required parameters, are described.

III. Battery Measurement

For this work a cell designed for automotive applications, the AHR32113M1 from A123 [20], is used. It is a commercial, cylindrical and high power Lithium-Ion cell being composed of an LFP (LiFePO4) cathode and a Graphite (G) anode. The operational parameters are summarised in Table I. The cell type, including other form factors, is popular for research in terms of modeling and testing [21]–[23]. It shows only minor degradation due to cycling [22] allowing for stable conditions during the test phase and over a wide SOC range.

Prior to the characterisation measurements three full cycles are conducted to compensate all reversible phenomena. Each cycle includes a 1 C constant current charge to the upper voltage limit of 3.6 V, a constant voltage phase at this limit until the current is dropping below 0.05 C, a resting period of 1 h, a discharge phase with 1 C to the lower voltage limit of 2.2 V and

TABLE I
Operational Parameters of the A123 AHR32113M1 Cell [20]

Dimensions	∅32 × 113 mm
Mass	205 g
Capacity	4.4 Ah
Energy	14.5 Wh
Nominal voltage	3.3 V
Discharge power	550 W
Operating temperature	−30 to 55 °C
Cycle life 1 C/1 C 100% DOD	>5000

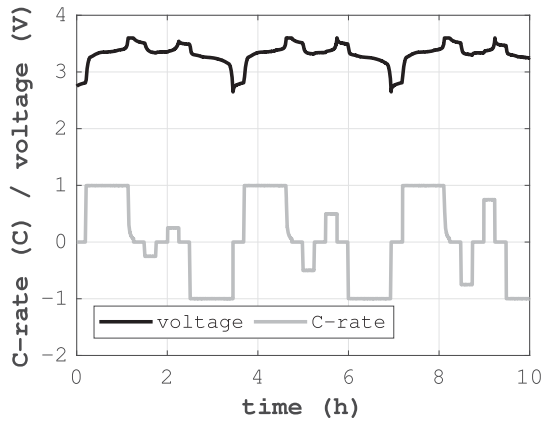

Fig. 2. Imposed cell current and resulting voltage profile during a measurement at 25 °C.

again a resting period of 1 h. Then, a capacity determination with full cycles is performed, whereas each second cycle delivers the nominal capacity used for the C-rate calculations in consequent cycles. A C-rate of 1 defines the current that has to be withdrawn from the battery so that it is discharged from SOC 1 to SOC 0 in one hour. For the characterisation itself, a profile is used which facilitates discharge and charge pulses with a current amplitude of 0.25 C, 0.5 C, 0.75 C, 1.00 C, 1.25 C, 1.50 C and a duration of 900 s each with a pause of 900 s in between. These current pulses are conducted from full charge (SOC 1) down to flat (SOC 0) in steps of 0.05. When voltage limits are reached during the test, the control mode changes from constant current to constant voltage. When the measurements at one SOC level are finished, a full discharge and charge cycle is performed and the next SOC level is set via discharge. Every measurement sequence is fully conducted at a temperature level of 0 °C, 25 °C, and 40 °C. Fig. 2 shows exemplary a part of the test sequence at 25 °C.

This profile aims at revealing the important aspects for this kind of simulation. The different values of the current allow averaging the over-voltages with respect to the current. The long pulses and breaks with a duration of 900 s each include the relevant time-dependent effects of double layer and diffusion both for load and relaxation and reveal the voltage hysteresis between charge and discharge. Nevertheless, only the rest periods are used for parameter extraction as the SOC does not change during these intervals. Different temperature levels reveal the dependency of the parameters on changes in temperature. Additionally, the full discharge and charge followed by reinitialising to SOC 1 and adjusting the SOC help to reduce the error of the SOC to a minimum.

IV. Algorithm for Parameter Estimation

The developed algorithm presented in this contribution uses measurement data for extracting the EEC parameters. First, the measured battery voltage is analysed in correlation with the imposed current steps. Based on the voltage reaction to the current and the different time constants of the RC-parallel circuits the parameters (OCV, R_s, R_{p1}, C_{d1}, R_{p2} and C_{d2}) can be estimated. In the next step, a PSO adjusts these parameters by utilising the differential equation of the circuit in order to find a configuration near the global optimum. Then, a GN algorithm uses the estimated parameters as start values and refines the extracted parameters. The optimisation algorithms thereby minimise the influence of measurement noise on the extracted battery parameters. Based on the knowledge that the optimisation problem is non-linear with respect to the parameters R_s, R_{p1}, C_{d1}, R_{p2} and C_{d2} it is reasonable to use a stochastic method as first step, because deterministic methods, which use the gradient of the optimisation function, can only find the nearest local optimum. Secondly, as refinement, the GN algorithm is used due to its fast convergence if the optimisation function can be assumed to be of quadratic shape, which is a good assumption if the starting value is already close to the optimum [24]. The combination of the PSO and the GN algorithms turns out to be a good trade-off between accuracy of the extracted parameters and calculation effort. Finally, the estimated parameters from the measurements at three different temperatures are combined in order to extract their correlation with temperature. In this contribution, only reversible effects in the battery are considered. Ageing effects such as loss of charge capacity or increase in internal impedance of the battery are hence neglected. Nevertheless, the variability of the parameters over time can be determined during long-time measurements if the characterisation of the battery is done in regular intervals. The following subsections give a more accurate insight into the different steps of the proposed algorithm.

A. Correlation Between Terminal Voltage and Current

At the beginning, the algorithm searches for steps greater than or equal to Δi_{min} in the current profile. Data below this minimum current step is considered to be measurement noise. The index values at the start of each step are stored in iStart. Next, the corresponding voltage trend after each current step is analysed. Based on the time constants τ_0, τ_1 and τ_2, and the respective height of the current step i_0, the voltage drops v_{Rs}, v_{Rp1} and v_{Rp2} over R_s, R_{p1} and R_{p2} respectively, are determined. The time constants thereby depend on the cell chemistry, temperature, SOC and state of health (SOH) [25] and must be chosen based on prior system knowledge and experimental data. After five times the time constant, the capacity of each RC-parallel circuit is considered to be fully charged. Hence the entire current flows over the respective resistance. This algorithm also introduces a fictitious time constant τ_0 for determining the value of R_s. This turned out to cause less errors for non-uniform sampling rates and rise-time caused by power electronics of the measurement equipment. The time constants which have been used for the LFP battery cell in this manuscript are provided in Table II. The chosen time constants also correspond to the values proposed by [19].

Algorithm 1: GetPar $(\Delta i_{min}, \tau_0, \tau_1, \tau_2)$.

for $j = 2$ to $size(t)$ **do**
  iStart $= find(\Delta \mathbf{i}_{meas}(j) >= \Delta i_{min})$
end for
for $k = 1$ to $size($**iStart**$)$ **do**
  iRs$(k) = find(\mathbf{t} == \mathbf{t}($**iStart**$(k) + 5 \cdot \tau_0)$
  iRp1$(k) = find(\mathbf{t} == \mathbf{t}($**iStart**$(k) + 5 \cdot \tau_1)$
  iRp2$(k) = find(\mathbf{t} == \mathbf{t}($**iStart**$(k) + 5 \cdot \tau_2)$
end for
$\mathbf{v}_{Rs} = \mathbf{v}_{meas}($**iRs**$) - \mathbf{v}_{meas}($**iStart**$)$
$\mathbf{v}_{Rp1} = \mathbf{v}_{meas}($**iRp1**$) - \mathbf{v}_{meas}($**iRs**$)$
$\mathbf{v}_{Rp2} = \mathbf{v}_{meas}($**iRp2**$) - \mathbf{v}_{meas}($**iRp1**$)$
$i_0 = \mathbf{i}_{meas}($**iStart**$) - \mathbf{i}_{meas}($**iStart** $- 1)$
SOC $= \mathbf{soc}_{meas}($**iRp2**$)$
OCV $= \mathbf{v}_{meas}($**iRp2**$)$
$\mathbf{R}_s = \frac{\mathbf{v}_{Rs}}{i_0}$
$\mathbf{R}_{p1} = \frac{\mathbf{v}_{Rp1}}{i_0}$
$\mathbf{R}_{p2} = \frac{\mathbf{v}_{Rp2}}{i_0}$
$\mathbf{C}_{d1} = \frac{\tau_1}{\mathbf{R}_{p1}}$
$\mathbf{C}_{d2} = \frac{\tau_2}{\mathbf{R}_{p2}}$
return $(\mathbf{SOC}, \mathbf{OCV}, \mathbf{R}_s, \mathbf{R}_{p1}, \mathbf{R}_{p2}, \mathbf{C}_{d1}, \mathbf{C}_{d2})$

TABLE II
Parameters of Algorithm 1

Threshold for current step	Δi_{min}	1 A
Fictitious ohmic time constant	τ_0	0.002 s
Short-term time constant	τ_1	4.5 s
Long-term time constant	τ_2	180 s

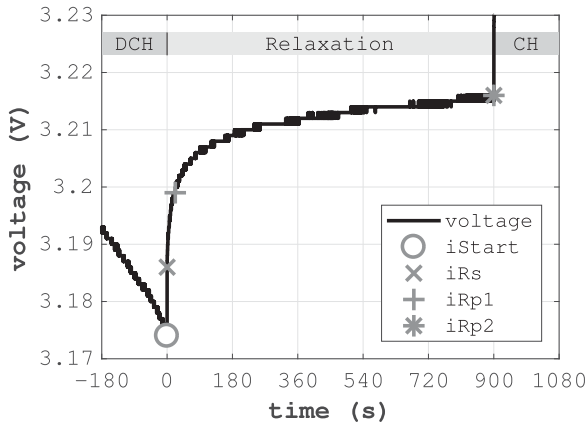

Fig. 3. Battery discharge (DCH) and charge (CH) with 0.75 C and relaxation phase (Relaxation) beginning at 0 s with the current switched off. Indices indicate the voltage drops at the respective resistances.

Fig. 3 depicts the relaxing battery voltage after discharging the battery with 0.75 C and then switching off the current at 0 s. Between 0 s and 900 s the battery voltage relaxes. After 900 s the battery is charged with 0.75 C. The observed bit-noise is only 1 mV and can therefore be neglected. The figure also shows the index values for iRs, iRp1 and iRp2. They represent the different voltage drops at the respective resistances of the

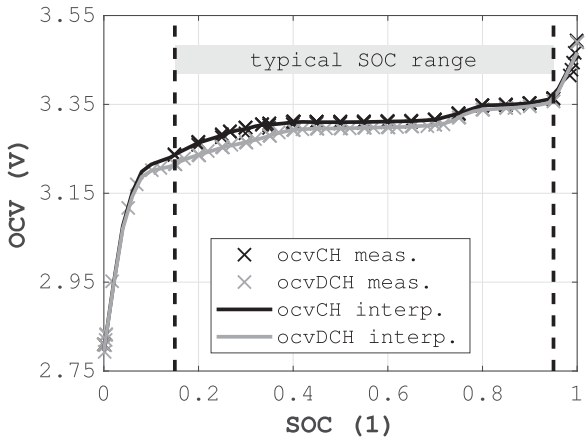

Fig. 4. OCV for charging (ocvCH) and discharging (ocvDCH) over SOC highlighting hysteresis determined from measurement and interpolated.

EEC model. The effects, which are described in chapter II can be observed between these indices. The ohmic voltage drop appears immediately after the current is switched off (iStart to iRs). The short-term effects (iRs to iRp1) within the range of seconds and the long-term effects (iRp1 to iRp2) within the range of minutes contribute to the relaxation effect [19].

The OCV is determined at the end of each relaxation phase. After a rest period of 900 s the change in voltage is below 0.015 mV/s, which can be interpreted as 'relaxed' state. Fig. 4 shows the measured and interpolated OCV for charging and discharging highlighting hysteresis at different SOC levels within the entire range from SOC 0 to SOC 1. The slopes show high correlation with the ones found in [26] where the values were estimated for the same type of cell but with another method. However, a better resolution of the curve could be achieved if the method were extended by measuring a continuous near idle OCV by discharging and charging the cell with a very low current.

Applying the ohmic law, the resistances are estimated based on the respective current step i_0 and the voltage drops. Finally, the capacities of the EEC can be calculated by dividing the time constants τ_1 and τ_2 by the already extracted corresponding resistances $\mathrm{R_{p1}}$ and $\mathrm{R_{p2}}$. The pseudocode for the described algorithm is presented in Algorithm 1.

B. Particle Swarm Optimisation

The PSO method [24] is a stochastic optimisation method and is based on observations of animals using swarm intelligence for optimal foraging. It implements the foraging system used by individuals within one swarm to mathematical equations in order to get close to the global optimum of the optimisation problem. One of the major strengths of this algorithm is that contrary to many deterministic methods (like the later discussed GN algorithm) the algorithm is more flexible and has the chance not only to reach the nearest local optimum but to get close to the global optimum.

The aim in this manuscript is to minimise the sum of the squared errors between simulated and measured voltage with respect to $\mathrm{R_s}$, $\mathrm{R_{p1}}$, $\mathrm{C_{d1}}$, $\mathrm{R_{p2}}$ and $\mathrm{C_{d2}}$. For each individual j the starting vector $(\Theta_0^j = ((\mathrm{R_s})_0^j, (\mathrm{R_{p1}})_0^j, (\mathrm{C_{d1}})_0^j, (\mathrm{R_{p2}})_0^j, (\mathrm{C_{d2}})_0^j)^T)$ and the starting velocity ($v_0^j \in \mathbb{R}^5$) of the PSO method are chosen completely randomly within a subspace of $\mathbb{R}^5$ respectively within $(0,1)^5 \subset \mathbb{R}^5$. However, in this work, the calculations of the previous step, described in Section IV-A, are used to set the initial values (Θ_0^j) randomly around the already calculated parameters. The advantage of this choice is that due to the large size of the intervals where the parameters can be located it takes less computation time to get the same accuracy than in the case where the starting values are equally distributed within $(L, R) \subset \mathbb{R}^5$. Keeping in mind that the feasible interval might not be equal for every parameter, the starting values should be chosen with respect to the size of the interval. Satisfiable results were achieved by setting

$$\Theta_0^j = \frac{(R-L)}{10^6}\mathrm{rand(5,1)} + \mathbf{a}, \tag{1}$$

where rand(5,1) denotes a five dimensional random vector with uniformly distributed values within $(0,1)$ (i.e., $\mathrm{rand(5,1)}_i \sim U(0,1)$ for $i = 1, ..., 5$), $\mathbf{a}$ symbolises the previously calculated parameters, $L \in \mathbb{R}^5$ denotes the lower bound and $R \in \mathbb{R}^5$ the upper bound of the feasible five dimensional interval.

Additionally, five constants, the number of individuals (N_{Ind}), inertia (ξ), two acceleration factors (c_1, c_2) and a tolerance value (ϵ) shall be chosen.

During the first iteration (i.e., $k = 0$) for each individual j the sum of the squared errors between simulated and measured voltage $E(j, 0)$ is calculated via

$$\mathrm{v_{sim}}(t, \Theta_0^j) = \mathrm{i_0}\left((\mathrm{R_s})_0^j + \gamma_1(t)(\mathrm{R_{p1}})_0^j + \gamma_2(t)(\mathrm{R_{p2}})_0^j\right) \tag{2}$$

where

$$\gamma_1(t) = 1 - \exp\left(\frac{-t}{\tau_1}\right),\ \gamma_2(t) = 1 - \exp\left(\frac{-t}{\tau_2}\right) \tag{3}$$

and

$$\tau_1 = (\mathrm{R_{p1}})_0^j(\mathrm{C_{d1}})_0^j,\ \tau_2 = (\mathrm{R_{p2}})_0^j(\mathrm{C_{d2}})_0^j. \tag{4}$$

Therefore, it holds that

$$E(j,0) = \sum_m (\mathrm{v_{sim}}(t_m, \Theta_0^j) - \mathrm{v_{meas}}(t_m))^2, \tag{5}$$

where $\mathrm{v_{meas}}(t_m)$ is the measured voltage at time t_m.
In the following step, the current 'best' individual $j^\star$ at position $\Theta_0^{j^\star}$ (i.e., $E(j^\star, 0) \leq E(i, 0)$ for all $i = 1, \ldots, N_{\mathrm{Ind}}$) is calculated. Set

$$E_{\mathrm{best}} = E(j^\star, 0) \text{ and } \Theta_{\mathrm{best}}^{\mathrm{global}} = \Theta_0^{j^\star}. \tag{6}$$

Additionally, for each individual the personal 'best' position (i.e., the position Θ_k^j, where $E(j,k)$ has the smallest values for individual j) should be stored (in the first iteration there is nothing to do), therefore $\Theta_{\mathrm{best}}^{\mathrm{pers}}(j) = \Theta_0^j$ and $E_{\mathrm{best}}^{\mathrm{pers}} = E(j,0)$ are set.

Assuming that $k-1$ iterations have been done, the iteration k is described as follows: Firstly, the position of individual j in iteration k is calculated

$$\Theta_k^j = \Theta_{k-1}^j + v_{k-1}^j, \tag{7}$$

where v_{k-1}^j is the velocity for individual j in step $k-1$. It should be noted that it has to be checked whether Θ_k^j still remains within

TABLE III
PARAMETERS OF ALGORITHM 2 AND 3

Number of individuals	N_{Ind}	10
Acceleration factor	c_1	2
Acceleration factor	c_2	2
Tolerance	ϵ	10^{-6}
Lower bound	L	$(10^{-5}, 10^{-5}, 1, 10^{-5}, 10)^T$
Upper bound	R	$(10^{-1}, 10^{-1}, 10^{5}, 10^{-1}, 10^{9})^T$

the feasible subspace of $\mathbb{R}^5$. In [27] a lot of suggestions for dealing with such a situation can be found. However, in this case it has turned out that the handling $\Theta_k^j = \min(\max(L, \Theta_k^j), R)$ was sufficient.

Secondly, for all new positions Θ_k^j the values $E(j,k)$ are calculated and compared with the current $\Theta_{\text{best}}^{\text{global}}$ and $\Theta_{\text{best}}^{\text{pers}}(j)$. If $E(j,k) < E_{\text{best}}$ then let $\Theta_{\text{best}}^{\text{global}} = \Theta_k^j$, if $E(j,k) < E_{\text{best}}^{\text{pers}}$ a new personal 'best' position is found.

Thirdly, based on knowledge of $\Theta_{\text{best}}^{\text{pers}}(j)$ and $\Theta_{\text{best}}^{\text{global}}$ a new velocity is calculated:

$$v_k^j = \xi v_{k-1}^j + c_1 X_1 \left(\Theta_{\text{best}}^{\text{pers}}(j) - \Theta_k^j\right) + c_2 X_2 \left(\Theta_{\text{best}}^{\text{global}} - \Theta_k^j\right) \tag{8}$$

with $X_i \sim U(0,1)$ for $i = 1, 2$. One can see that with greater distances to $\Theta_{\text{best}}^{\text{pers}}(j)$ and $\Theta_{\text{best}}^{\text{global}}$, individual j is more likely to have a greater velocity than individuals with smaller distances.

Following a suggestion in [28], setting ξ not only as a constant, but

$$\xi_k = 1 - \frac{0.8\,k}{N_{\max}} \text{ and } \xi_0 = 1, \tag{9}$$

with $N_{\max}$ denoting the maximal number of iterations, led to a greater accuracy.

Table III shows the parameter values used in the implementation of the PSO method. Experiments proved that concerning accuracy and calculation speed the acceleration factors c_1 and c_2 are highly sensitive regarding the input data, which is also mentioned in [24]. In this implementation c_1 and c_2 were chosen following a suggestion in [27], which worked well for all input data used in this work. However, there might be better choices for different inputs due to the sensitivity of these parameters. The pseudocode for the implemented PSO is shown in Algorithm 2.

Algorithm 2: PSO $(N_{\text{Ind}}, c_1, c_2, \epsilon, N_{\max})$.

while $k < N_{\max}$ **and** $E_{\text{best}} > \epsilon$ **do**
  $k = k + 1$
  for $j = 1$ **to** N_{Ind} **do**
    $\Theta_k^j = \Theta_{k-1}^j + v_{k-1}^j$
    calculate $E(j,k)$
    if $E(j,k) < E_{\text{best}}$ **then**
      $E_{\text{best}} = E(j,k)$
      $\Theta_{\text{best}}^{\text{global}} = \Theta_k^j$
    end if
    if $E(j,k) < E_{\text{best}}^{\text{pers}}$ **then**
      $E_{\text{best}}^{\text{pers}} = E(j,k)$
      $\Theta_{\text{best}}^{\text{pers}}(j) = \Theta_k^j$
    end if
    $\text{diff}_{\text{p}} = \Theta_{\text{best}}^{\text{pers}}(j) - \Theta_k^j$
    $\text{diff}_{\text{g}} = \Theta_{\text{best}}^{\text{global}} - \Theta_k^j$
    $X_1 = \text{rand}()$
    $X_2 = \text{rand}()$
    $v_k^j = \xi v_{k-1}^j + c_1 X_1 \text{diff}_{\text{p}} + c_2 X_2 \text{diff}_{\text{g}}$
    $\xi = 1 - \frac{0.8k}{N_{\max}}$
  end for
end while
return $(\Theta_{\text{best}}^{\text{global}})$

C. Gauss-Newton Algorithm

The idea of the GN algorithm [24], [29], which is a nonlinear regression method, is, using a second-order Taylor approximation in order to get close to a minimum of the squared error function.

Analogously to the previous section, the parameter vector can be defined as $\Theta = (\text{R}_\text{s}, \text{R}_{\text{p1}}, \text{C}_{\text{d1}}, \text{R}_{\text{p2}}, \text{C}_{\text{d2}})^T \in \mathbb{R}^5$. The residual $r(\Theta)$ is defined as

$$r(\Theta) = (\text{v}_{\text{sim}}(\mathbf{t}, \Theta) - \text{v}_{\text{meas}}) \in \mathbb{R}^M, \tag{10}$$

with $\mathbf{t} \in \mathbb{R}^M$ denoting the time vector of the measurement and v_{sim} defined in (2).

The regression problem is described as:

$$\text{Find } \Theta^\star \text{ with } \|r(\Theta^\star)\|_2^2 = \min_{\Theta} \|r(\Theta)\|_2^2, \tag{11}$$

where $\|x\|_2 = \sqrt{x^T x}$ denotes the Euclidean norm. The regression problem (11) is therefore equivalent to the minimisation of $f(\Theta) = \frac{1}{2} r(\Theta)^T r(\Theta)$. A second order Taylor approximation with respect to f yields

$$f(\Theta) \approx f(\hat{\Theta}_k) + \text{grad}_f^T(\hat{\Theta}_k)(\Theta - \hat{\Theta}_k) + \frac{1}{2}(\Theta - \hat{\Theta}_k)^T \mathbf{H}_f(\hat{\Theta}_k)(\Theta - \hat{\Theta}_k), \tag{12}$$

with the Hessian matrix $(\mathbf{H}_f)_{ij} = \left(\frac{\partial^2 f}{\partial\Theta_i \partial\Theta_j}\right)_{ij} \in \mathbb{R}^{5\times 5}$ for $i, j = 1, ..., 5$.

In order to find the difference $(\Theta - \hat{\Theta}_k)$, where $f(\Theta)$ is minimal, we get the necessary condition that

$$\mathbf{0} = \frac{\partial f}{\partial(\Theta - \hat{\Theta}_k)} \approx \text{grad}_f(\hat{\Theta}_k) + \mathbf{H}_f(\hat{\Theta}_k)(\Theta - \hat{\Theta}_k), \tag{13}$$

which yields the equation

$$\begin{aligned} \Theta &\approx \mathbf{H}_f(\hat{\Theta}_k)^{-1}\left(-\text{grad}_f(\hat{\Theta}_k) + \mathbf{H}_f(\hat{\Theta}_k)(\hat{\Theta}_k)\right) \\ &\approx \hat{\Theta}_k - \mathbf{H}_f(\hat{\Theta}_k)^{-1}\text{grad}_f(\hat{\Theta}_k). \end{aligned} \tag{14}$$

Therefore, we set

$$\hat{\Theta}_{k+1} = \hat{\Theta}_k - \mathbf{H}_f(\hat{\Theta}_k)^{-1}\text{grad}_f(\hat{\Theta}_k). \tag{15}$$

Keeping in mind that $f(\Theta) = \frac{1}{2}\sum_{\ell=1}^M r_\ell(\Theta)^2$, it follows that

$$\left(\text{grad}_f(\Theta)\right)_i = \sum_{\ell=1}^{M} \frac{\partial r_\ell}{\partial\Theta_i}(\Theta) r_\ell(\Theta) \text{ for } i = 1, \ldots, 5. \tag{16}$$

Algorithm 3: GN $(\epsilon, N_{\max})$.

for $k = 1$ to $N_{\max}$ **do**
  $r =$ residual $r(\hat{\Theta}_k)$
  $J =$ Jacobian $r(\hat{\Theta}_k)'$
  $\hat{\Theta}_{k+1} = \hat{\Theta}_k - (J^T J)^{-1} J^T r$
  if $r(\hat{\Theta}_k) < r(\hat{\Theta}_{k-1})$ **then**
    $\Theta^\star = \hat{\Theta}_k$
  end if
  if $r(\hat{\Theta}_{k-1}) < \epsilon$ **then**
    break
  end if
  return $(\Theta^\star)$
end for

TABLE IV
COMPUTATION TIME GN, PSO AND PSO&GN

GN	12.112 s	11.856 s	12.143 s
PSO*	24.209 s	24.606 s	24.198 s
PSO&GN	24.996 s	24.974 s	25.151 s

This result can be written as $\text{grad}_f(\Theta) = [r(\Theta)']^T\, r(\Theta)$, where $r(\Theta)'$ denotes the Jacobian matrix of r at point Θ.

The Hessian matrix is calculated the following way

$$(\mathbf{H}_f(\Theta))_{ij} = \sum_{\ell=1}^{M} \frac{\partial r_\ell}{\partial \Theta_i} \frac{\partial r_\ell}{\partial \Theta_j}(\Theta) + \sum_{\ell=1}^{M} \frac{\partial^2 r_\ell}{\partial \Theta_i \partial \Theta_j} r_\ell(\Theta), \quad (17)$$

for $i, j = 1, \ldots, 5$.

Assuming that $r_\ell(\Theta^\star) \ll 1$, the second sum in (17) vanishes for Θ sufficiently close to $\Theta^\star$. In summary, the GN algorithm is

$$\hat{\Theta}_{k+1} = \hat{\Theta}_k - \left(\left[r(\hat{\Theta}_k)' \right]^T r(\hat{\Theta}_k)' \right)^{-1} \cdot \left[r(\hat{\Theta}_k)' \right]^T r(\hat{\Theta}_k). \quad (18)$$

Due to the fact that equation (13) is only a necessary condition, one can not be sure whether the result is a saddle point, a maximum or a minimum. Besides, the algorithm does not distinguish between global or local extrema. Additionally, the residual r is a nonlinear function with respect to Θ and therefore the second order approximation might not be precise enough if the value Θ is not close to the minimum.

As a matter of fact, it is reasonable to use the GN algorithm only after the previously described PSO method, because then the starting value should be close enough to the global minimum, where the function r can be assumed to be of quadratic shape. The pseudocode for the implemented GN algorithm is presented in Algorithm 3.

D. Comparison of the Optimisation Algorithms

This subsection provides a short comparison of GN, PSO and the suggested combination of both algorithms (PSO&GN) regarding computation time and accuracy. Table IV shows the elapsed time of the three algorithms applied on the presented problem (430 optimisation problems were solved in every single run). For each algorithm three runs were performed. PSO* means that N_{Ind} is set to 20 instead of 10 in order to reduce the squared error while keeping the computation costs similar to the suggested algorithm.

TABLE V
SQUARED ERROR GN, PSO AND PSO&GN

GN	$1.785 \cdot 10^{-5}$ V^2	$1.780 \cdot 10^{-5}$ V^2	$1.815 \cdot 10^{-5}$ V^2
PSO*	$1.895 \cdot 10^{-5}$ V^2	$1.895 \cdot 10^{-5}$ V^2	$1.895 \cdot 10^{-5}$ V^2
PSO&GN	$8.198 \cdot 10^{-6}$ V^2	$8.436 \cdot 10^{-6}$ V^2	$8.377 \cdot 10^{-6}$ V^2

Table V shows the sum of the squared errors between simulated and measured voltage as described in the sections above. For each of the three runs the mean value of the 430 optimisation problems is shown.

One can see that using only a GN algorithm for the model problem leads to low computation costs, because the algorithm converges fast to the nearest local optimum. As Algorithm 1 calculates appropriate start values for the optimisation algorithms, the risk of running into a local minimum is decreased. However, the squared error of the GN algorithm can be significantly improved by using the PSO&GN algorithm while the computation time only doubles. Additionally, it can be seen that it is more efficient to use a PSO method with a rather small number of individuals in order to get close to the global optimum and afterwards a GN routine for refinement than to use a PSO method with more individuals.

E. Temperature Dependency of the Parameters

Measurements are performed at three different temperatures. Therefore, battery parameters can be extracted varying with SOC but they are only valid at the three distinct measured temperatures. However, during simulations the battery cell also reaches temperatures different to the measured ones and therefore an additional dependency of the EEC parameters on any temperature T has to be considered and implemented. For a more flexible implementation a functional approach is preferred over a look-up table. Here, the determination of the dependency function is exemplary shown for the series resistance of the battery cell. Any three or more temperatures can be chosen, but in the case of a conditioned automotive or stationary battery application, 0 °C, 25 °C and 40 °C reflect the thermal operation window well. For the extraction process a reference SOC is defined, which is 0.6 in this contribution because it is within the commonly usable range of around SOC 0.15 to SOC 0.95 for (plug-in) electric vehicles [30], indicated in Fig. 5 by the vertical line. At this SOC the differences $\text{R}^{0.6}_{25\text{-}0} = \text{R}^{0.6}_{25} - \text{R}^{0.6}_{0}$ and $\text{R}^{0.6}_{25\text{-}40} = \text{R}^{0.6}_{25} - \text{R}^{0.6}_{40}$ are determined. Then, three nodes are defined by

$$\kappa(\text{T}) = \begin{cases} -\frac{\text{R}^{0.6}_{25\text{-}0}}{\text{R}^{0.6}_{25\text{-}40}} : \text{T} = 0\,^\circ\text{C} \\ 0 : \text{T} = 25\,^\circ\text{C} \\ -1 : \text{T} = 40\,^\circ\text{C} \end{cases} \quad (19)$$

and used for fitting a gain-function κ, which conforms with the exponential temperature dependency of chemical processes described by Arrhenius' law [31], [32]. This functions allows to calculate the resistance over the whole temperature range also at temperatures that have not been measured, as depicted

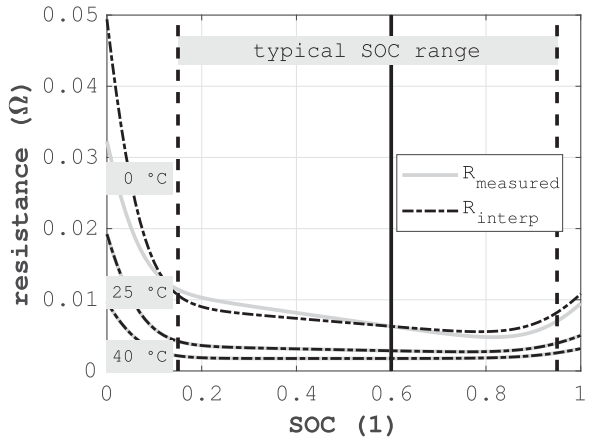

Fig. 5. Comparison of the measured and the interpolated series resistance of the cell at 0 °C, 25 °C and 40 °C. The vertical line at SOC 0.6 denotes the chosen reference SOC.

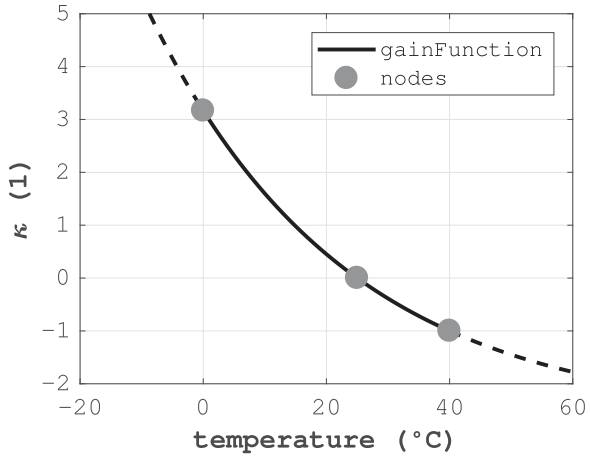

Fig. 6. Gain values of the series resistance including the nodes of the temperature dependency function.

in Fig. 6. The actual resistance for any temperature and SOC is calculated based on the resistance difference between the two distinct temperatures 25 °C and 40 °C denoted as $R_{25–40}$

$$R(SOC, T) = R_{25}(SOC) + \kappa(T)R_{25–40}(SOC). \tag{20}$$

This interpolation method yields a good correlation to the measured values as depicted in Fig. 5 and both the temperature and the SOC dependency correspond with expectations for LFP cells [25]. As the temperature dependency is calculated based on the measurements at 40 °C and 25 °C, compare (20), these curves fit exactly to the measurements while values at other temperatures, like the 0 °C line, are calculated values. However, at reference SOC 0.6 and adjacent areas the three interpolated curves correspond closely to the measured curves.

V. Validation

As the correlation between the parameters of the EEC and the SOC as well as the battery temperature are now estimated, they can be used to simulate the operating behaviour of the representative LFP battery cell. The comparison of the measurements with the simulated battery voltage during a dynamic current profile allows for determining the accuracy and reliability of the generated parameter set.

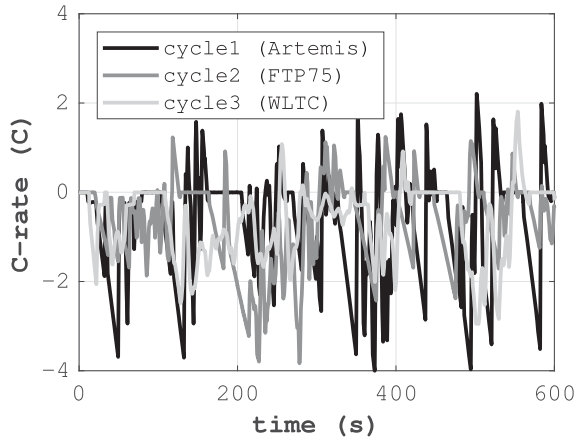

Fig. 7. First 600 s of dynamic current profiles (based on real-life driving cycles), which have been used for validation.

Three dynamic current profiles have been derived from standardised real-life automotive driving cycles (Artemis, FTP75 and WLTC) for validating the simulated operating behaviour of the battery. Therefore, an already validated vehicle model [33] of a Mitsubishi i-MiEV is used to extract the required battery current during the three driving cycles. Then, these current profiles are scaled to a maximum of 4 C (for charging or discharging) in order not to exceed the maximum current rate recommended by the manufacturer of the cells. Fig. 7 shows the first 600 s of the extracted current profiles.

The three current profiles have been repeatedly applied to the fully charged LFP cells until the lower voltage level was reached. In addition, the same load current was applied to the battery model in the simulation environment. This allows for objective evaluation of the estimated battery parameters within the entire SOC range. Furthermore, the evaluation has been conducted at two different temperatures, 10 °C and 35 °C. As the parameters have been extracted at 0 °C, 25 °C and 40 °C, the chosen temperatures enable a fair evaluation of the extracted temperature dependency.

Fig. 8 shows the results of the validation. The relative error between the simulated and measured battery voltage is provided over the SOC for all six validation scenarios. The relative voltage error is calculated based on

$$\text{relative error} = 100 \cdot \frac{v_{meas} - v_{sim}}{v_{meas}}. \tag{21}$$

The results prove that the extracted parameters are capable of reproducing the real battery behaviour accurately from SOC 0.15 to SOC 0.95. The maximum deviation in this interval remains below 34 mV which is 1.09% of the terminal voltage. Below this interval, from SOC 0 to SOC 0.15, the highest deviation occurs. Here, the voltage error reaches its maximum value of 21.35%. This can be explained by the fact that the battery has a strongly non-linear behaviour over its SOC, especially outside the range of SOC 0.15 to SOC 0.95, and is therefore hard to model with the proposed linear EEC which, in this case, is optimised to obtain high accuracy over the biggest region possible.

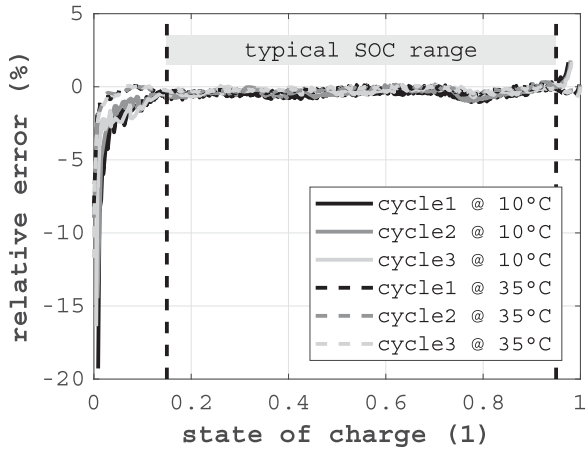

Fig. 8. Relative error between simulated and measured battery voltage within the entire SOC range.

TABLE VI
ABSOLUTE VALUE OF THE MAXIMUM RELATIVE VOLTAGE ERROR IN DIFFERENT APPLICATION SCENARIOS

Cycle/temperature	**1/10 °C**	**2/10 °C**	**3/10 °C**
SOC 0 - SOC 0.15	19.27%	14.47%	16.38%
SOC 0.15 - SOC 0.95	1.09%	0.98%	0.74%
SOC 0.95 - SOC 1	1.68%	1.80%	1.61%
cycle/temperature	**1/35 °C**	**2/35 °C**	**3/35 °C**
SOC 0 - SOC 0.15	16.88%	16.65%	21.35%
SOC 0.15 - SOC 0.95	0.62%	0.59%	0.52%
SOC 0.95 - SOC 1	0.16%	0.13%	0.01%

Within the interval SOC 0.95 to SOC 1 the maximum deviation is 1.8%. Table VI summarises the maximum relative voltage error in each of the three scenarios at both temperatures within each of the described SOC intervals, respectively.

The papers [26] and [30] claim that usually not the entire available range from SOC 0 to SOC 1 is allowed by the Battery Management System (BMS) due to safety and reliability aspects. On the one hand, below SOC 0.15, the battery cannot deliver a stable voltage due to the strongly decreasing OCV at these SOC levels (compare also Fig. 4). On the other hand, considering an entirely charged battery at a charge level higher than SOC 0.95, the battery degradation would be unnecessarily high because of increased chemical side reactions [31], [32]. Hence, a BMS usually tries to keep the SOC within the interval SOC 0.15 and SOC 0.95 [30], in order to enable stable operation and to increase the cycle life of the battery. The findings in the validation section have already proven that the battery model is capable of reproducing the battery operating behaviour in this SOC interval accurately. The SOC levels where the battery model shows higher voltage errors (i.e., SOC 0 to SOC 0.15 and SOC 0.95 to SOC 1) are hence not relevant under typical operating conditions.

To give an example, in automotive applications a serial connection of about 120 LFP battery cells leads to a battery stack voltage of around 400 V. If we now assume the maximum deviation of 34 mV per cell that occurred within SOC 0.15 and SOC 0.95, this would mean only 4.08 V deviation on stack level, which is accurately enough for most applications.

VI. CONCLUSION AND OUTLOOK

This manuscript has presented a comprehensive algorithm for determining battery parameters of a Lithium-Ion battery from measurements. The algorithm estimates the parameters based on time constants and the observed transient voltage trend, which is correlated to the respective current steps of a measurement profile. In the next step, a two-level optimisation routine is used to fit the estimated parameters further to the measurement. Therefore, a PSO is used to find the global optimum of the parameters. Subsequently, a GN algorithm takes care of the fine tuning, in order to further improve the extracted parameters. In the next step, the parameters are correlated with the battery temperature. Finally, the extracted parameter set is validated using a dynamic current profile.

The validation showed that the simulated operating behaviour correlates with the real measured behaviour. The maximum deviation between the simulated and the measured terminal voltage of the battery remains below 34 mV or 1.09% within the typical operating range of an electric vehicle's battery, which is usually between SOC 0.15 and SOC 0.95.

Future research activities in this field will focus on decreasing the required time for the entire work-flow. This includes both the measurement procedure and the algorithm. Additionally, further improving the generated parameter set for achieving even more accurate and reliable simulation results will be targeted. Exemplary, a more accurate OCV curve could be achieved by discharging and charging the cell with a very low current while acquiring the terminal voltage continuously.

Regarding the GN algorithm, due to the approximation of the Hessian matrix some accuracy is lost. Additional testing will have to be done in order to find out if other deterministic algorithms with similar or even less calculation effort would lead to even better results.

REFERENCES

[1] M. Greenleaf, O. Dalchand, H. Li, and Z. J. P., "A temperature-dependent study of sealed lead-acid batteries using physical equivalent circuit modeling with impedance spectra derived high current/power correction," *IEEE Trans. Sustain. Energy*, vol. 6, no. 2, pp. 380–387, Apr. 2015.

[2] P. Malysz, J. Ye, R. Gu, H. Yang, and A. Emadi, "Battery state-of-power peak current calculation and verification using an asymmetric parameter equivalent circuit model," *IEEE Trans. Veh. Technol.*, vol. 65, no. 2, pp. 4512–4522, Jun. 2015.

[3] C. Blanco *et al.*, "An equivalent circuit model with variable effective capacity forlifepo4 batteries," *IEEE Trans. Veh. Technol.*, vol. 63, no. 8, pp. 3592–3599, Oct. 2014.

[4] D. Dvorak, T. Bäuml, H. Kapeller, and D. Simic, "Developing, modeling and validating multi physics battery models," in *Proc. 16th ITI Conf. Symp.*, ITI GmbH Dresden, Dresden, Germany, 2013, pp. 146–152.

[5] O. Tremblay, L. Dessaint, and A. Dekkiche, "A generic battery model for the dynamic simulation of hybrid electric vehicles," *Veh. Power Propulsion Conf.*, vol. 1, pp. 284–289, 2007.

[6] M. Chen and G. Rincon-Mora, "Accurate electrical battery model capable of predicting runtime and I-V performance," *IEEE Trans. Energy Convers.*, vol. 21, no. 2, pp. 504–5011, Jun. 2006.

[7] P. M. Gomadam, J. W. Weidner, R. A. Dougal, and R. E. White, "Mathematical modeling of lithium-ion and nickel battery systems," *J. Power Sources*, vol. 110, pp. 267–284, 2002.

[8] A. Jossen and W. Weydanz, *Moderne Akkumulatoren Richtig Einsetzen*, vol. 1. Basel, Switzerland: Reichardt Verlag, 2006.

[9] S. Buller, "Impedance-based simulation models for energy storage devices in advanced automotive power systems," Ph.D. dissertation, Rheinisch-Westflische Technische Hochschule Aachen, Aachen, Germany, 2002.

[10] W. Waag, C. Fleischer, and D. U. Sauer, "Critical review of the methods for monitoring of lithium-ion batteries in electric and hybrid vehicles," *J. Power Sources*, vol. 258, pp. 321–339, 2014.
[11] T. Kim, W. Qiao, and L. Qu, "Real-time state of charge and electrical impedance estimation for lithium-ion batteries based on a hybrid battery model," in *Proc. 28th Annu. IEEE Appl. Power Electron. Conf. Expo.*, Mar. 2013, pp. 563–568.
[12] W. Xian, B. Long, M. Li, and H. Wang, "Prognostics of lithium-ion batteries based on the Verhulst model, particle swarm optimization and particle filter," *IEEE Trans. Instrum. Meas.*, vol. 63, no. 1, pp. 2–17, Jan. 2014.
[13] C. Hu *et al.*, "Data-driven method based on particle swarm optimization and k-nearest neighbor regression for estimating capacity of lithium-ion battery," *Appl. Energy*, vol. 129, pp. 49–55, 2014.
[14] M. A. Rahman, S. Anwar, and A. Izadian, "Electrochemical model parameter identification of a lithium-ion battery using particle swarm optimization method," *J. Power Sources*, vol. 307, pp. 86–97, 2016.
[15] S. Li and X. Cheng, "A comparative study on rc models of lithium-ion battery," in *Proc. IEEE Conf. Expo Transp. Electrification Asia-Pac.*, Aug. 2014, pp. 1–4.
[16] V. Ramadesigan *et al.*, "Parameter estimation and capacity fade analysis of lithium-ion batteries using first-principles-based efficient reformulated models," *ECS Trans.*, vol. 19, no. 16, pp. 11–19, 2009.
[17] J. Reuter, E. Mank, H. Aschemann, and A. Rauh, "Battery state observation and condition monitoring using online minimization," in *Proc. 21st Int. Conf. Methods Models Autom. Robot.*, Aug. 2016, pp. 1223–1228.
[18] W.-J. Shen and H.-X. Li, "Multi-scale parameter identification of lithium-ion battery electric models using a PSO-LM algorithm," *Energies*, vol. 10, no. 4, pp. 1–18, 2017.
[19] A. Li, S. Pelissier, P. Venet, and P. Gyan, "Fast characterization method for modeling battery relaxation voltage," *Batteries*, vol. 2, pp. 1–15, 2016.
[20] "High Power AHR32113 Cylindrical Cell," [Online]. Available: http://www.a123systems.com/32113-lithium-iron-phosphate-high-power-batt%eries.htm, Accessed on: Mar. 3, 2017.
[21] M. Mastali *et al.*, "Battery state of the charge estimation using kalman filtering," *J. Power Sources*, vol. 239, pp. 294–307, 2013.
[22] M. Held and U. Sennhauser, "Stress-induced ageing of lithium-ion batteries," *CHIMIA Int. J. Chem.*, vol. 69, no. 12, pp. 737–740, 2015.
[23] N. Jayasekara, M. A. S. Masoum, and P. J. Wolfs, "Optimal operation of distributed energy storage systems to improve distribution network load and generation hosting capability," *IEEE Trans. Softw. Eng.*, vol. 7, no. 1, pp. 250–261, Jan. 2016.
[24] D. Schröder, *Intelligente Verfahren: Identifikation und Regelung nichtlinearer Systeme*. Berlin, Germany: Springer, 2010.
[25] W. Waag, S. Kbitz, and D. U. Sauer, "Experimental investigation of the lithium-ion battery impedance characteristic at various conditions and aging states and its influence on the application," *Appl. Energy*, vol. 102, pp. 885–897, 2013.
[26] T. Huria, G. Ludovici, and G. Lutzemberger, "State of charge estimation of high power lithium iron phosphate cells," *J. Power Sources*, vol. 249, pp. 92–102, 2014.
[27] K. E. Parsopoulos and M. N. Vrahatis, "Particle swarm optimization method for constrained optimization problem," *Frontiers Artif. Intell. Appl.*, vol. 76, pp. 214–220, 2002.
[28] M. Pluhacek, R. Senkerik, D. Davendra, Z. Kominkova Oplatkova , and I. Zelinka, "On the behavior and performance of chaos driven PSO algorithm with inertia weight," *Comput. Math. Appl.*, vol. 66, pp. 122–134, 2013.
[29] R. W. Freund and R. H. W. Hoppe, *Stör/Burlisch: Numerische Mathematik 1*, 10th ed. Berlin, Germany: Springer, 2007.
[30] A. Poullikkas, "Sustainable options for electric vehicle technologies," *Renew. Sustain. Energy Rev.*, vol. 41, pp. 1277–1287, 2015.
[31] Y. Yang, X. Hu, D. Qing, and F. Chen, "Arrhenius equation-based cell-health assessment: Application to thermal energy management design of a HEV NiMH battery pack," *Energies*, vol. 6, no. 5, pp. 2709–2725, 2013.
[32] B. Y. Liaw *et al.*, "Correlation of arrhenius behaviors in power and capacity fades with cell impedance and heat generation in cylindrical lithium-ion cells," *J. Power Sources*, vol. 119–121, pp. 874–886, 2003.
[33] D. Simic *et al.*, "Modeling and validation of lithium-ion battery based on electric vehicle measurement," Tech. Paper 2014-01-1850, 2014.

Dominik Dvorak received the M.Sc. degree in mechatronics/robotics from the University of Applied Science Vienna, Vienna, Austria, in 2013. Since 2013, he has been a Researcher with the business unit Electric Drive Technologies, AIT Austrian Institute of Technology GmbH, Vienna, Austria. His research interests includes algorithm development, thermal management and energy management for automotive- and aircraft-electromobility applications as well as modeling and simulation of these systems and its components.

Thomas Bäuml received the DI(FH) degree in mechatronics from the University of Applied Sciences Wiener Neustadt, Neustadt, Austria, in 2005. Since January 2006, he has been a Research Associate with the business unit Electric Drive Technologies, AIT Austrian Institute of Technology GmbH, Vienna, Austria. His research interests include thermal and electrical battery simulations, vehicle thermal- and energy management and longitudinal, and lateral dynamic vehicle simulations. Since 2007, he has been a Member of the Modelica Association (www.modelica.com).

Alexandra Holzinger received the B.Sc. degree in technical mathematics in 2016 from the Technical University of Vienna, Vienna, Austria. She is currently working toward the M.Sc. degree in applied mathematics. In summer 2016, she served an internship with the AIT Austrian Institute of Technology GmbH, Vienna, Austria. Thereby, she worked on mathematical optimisation methods for electrochemical system identification and state of charge estimation methods.

Hartmut Popp received the B.Sc. and M.Sc. degrees in industrial electronics from FH Technikum Vienna, Vienna, Austria and the Dipl.-Ing. degree in environment and bioresources management from the BOKU University Vienna, Vienna, Austria. Since 2017, he has been working toward the Ph.D. degree at the Institute of Electronic Sensor Systems, Technical University Graz, Graz, Austria. After working as a Design Engineer for Industrial Power Supplies, Siemens AG Vienna, he joined the AIT Austrian Institute of Technology GmbH in 2009. His research interests include testing, modeling and diagnostics of Lithium-Ion batteries.